Process Design of a Multistage Drying Process via Flowsheet Simulation

Moritz Buchholz[1,*], Johannes Haus[2], Lukas Blesinger[2], Christian Riemann[2], Swantje Pietsch[1], Frank Kleine Jäger[2], and Stefan Heinrich[1]

DOI: 10.1002/cite.202000207

Multistage drying processes including spray drying and fluidized bed unit operations are challenging to design due to the dependencies of the preceding process steps. Flowsheet simulation offers the possibility to simulate a complete process by the application of suitable short-cut models. In this contribution a novel model for a spray dryer based on a population balance approach is presented. Furthermore, a dynamic model for a fluidized bed dryer is introduced. Experimental data is used for validation and parameter optimization. The calibrated models are then used to design an industrial drying process of multiple drying stages.

Keywords: Dynamic modeling, Flowsheet simulation, Fluidized bed, Population balance, Spray drying

Received: September 18, 2020; *accepted:* February 04, 2021

1 Introduction

Spray towers are widely applied in the production of chemicals, e.g., catalysts or substances for protection of crops, as well as various food powders. On production scale, a second drying stage is often required due to limited residence times inside the spray dryer to reach the desired low moisture contents. This mainly occurs for temperature-sensitive materials, which must not experience high temperatures, especially in the inlet region. In this combination, the solids formulation and parts of the drying is carried out in the spray column, whereas the long residence time needed for final drying is guaranteed by the following fluidized bed dryer. To establish better control of the moisture content out of the coupled spray drying and fluidized bed drying process, the fluidized bed chamber may be divided into several subsequent drying chambers.

In such interconnected systems, the dimensioning and optimization of the single unit operations becomes difficult without considering the time dynamic behavior of previous and ensuing process steps. To allow for a consideration of the interdependencies of the single unit operations, flowsheet models can be used by simulation of the whole process, including recycle streams. Although flowsheet simulation is state of the art for processes containing purely fluid materials, the dynamic simulation of solids processes is still challenging, mainly due to the granularity of the considered material properties [1]. These issues are tackled by the novel open-source simulation framework Dyssol (acronym for dynamic simulation of solids processes), which is used in this contribution [1]. Dyssol inherently gives the option to keep track of the multidimensional distributed properties of particulate materials, like particle size distributions and moisture contents, in a time-dynamic simulation setting. Dyssol uses a sequential-modular approach in combination with partitioning and tearing methods to solve complex flowsheets including recycle streams. An extensive overview of the applied methods and algorithms is given by [2].

Common approaches for the development of shortcut models for spray drying processes revolve around plug flow or ideal mixing considerations. Birchal and Passos [3] chose the approach of an ideally mixed reactor to compute the time dynamic behavior of a spray drying process for milk powder production. The model considers particles with different residence times and therefore allows for the distinction between the evaporation processes of droplets and already solidified particles. Petersen et al. [4] presented a shortcut model for a spray dryer with serially connected fluidized bed units, based on physically derived balances and empirical approaches. However, the granular phase is only resolved for a characteristic diameter, such that the change in the size distribution of the granules cannot be observed in detail. Ali et al. [5] described a one-dimensional plug-flow model of a countercurrent spray drying process for

[1]Moritz Buchholz, Dr.-Ing. Swantje Pietsch, Prof. Dr.-Ing. Stefan Heinrich
moritz.buchholz@tuhh.de
Hamburg University of Technology, Institute of Solids Process Engineering and Particle Technology, Denickestraße 15, 21073 Hamburg, Germany.

[2]Dr.-Ing. Johannes Haus, Lukas Blesinger, Christian Riemann, Prof. Dr.-Ing. Frank Kleine Jäger
BASF SE, Solids formulation and handling/Digitalization of R&D – L540, Carl-Bosch-Straße 38, 67056 Ludwigshafen, Germany.

detergent production. The stationary state of the spray dryer is computed by simplified calculation of particle velocities and the resulting heat and mass transfer with the hot gas.

A series of modeling approaches for fluidized bed drying can be found in literature, which vary in the degree of abstraction in which the hydrodynamics are considered and how the particle size and moisture distribution are treated. Gnielinksi et al. [6] calculated the moisture change of particles in a batch fluidized bed dryer via an overall moisture balance over inlet and outlet gas. Palancz [7] included a two-phase model for the bubbling fluidized bed hydrodynamics. The energy and mass transport between bubbles and suspension is, hence, dependent on operation parameters like gas temperature and fluidization velocity. Lai et al. [8] extended this model by introducing a resistance for the evaporation from the particle surface. Additionally, the bubble gas is considered with a plug flow like behavior meaning that the heat and mass transport between suspension and bubble is calculated along the fluidized bed dryer height. Garnavi et al. [9] included changing bubble sizes along the dryer height, which corresponds more to the general understanding of bubbling fluidized beds. More recently, population-based models are used to describe the drying in fluidized beds to keep tracking of the drying for particles of different size possible [10–12].

In this contribution, a novel spray dryer model based on a two-dimensional population balance approach to describe the dynamic evolution of droplet and particle evaporation is presented. Additionally, a dynamic model for a fluidized bed unit operation is introduced. Both models are validated based on lab and pilot-scale experiments and show promising results regarding the description of both drying mechanisms and dynamic behavior. The models are then connected in a multistage drying process and simulated using the flowsheet simulation framework Dyssol to show the viability of this approach for process design and plant optimization purposes.

2 Framework Models

2.1 Spray Dryer

The spray drying process under consideration is operated in cocurrent mode. The present model uses a well-mixed approach to account for the changing gas and granular states inside the drying chamber. The droplet size distribution at the inlet is prescribed by a normal distribution. In the drying chamber, the droplets dry and solidify showing different drying behavior that is usually described by two distinct drying stages. During the first drying stage, the drop size shrinks and the contained primary particles move towards the drop's center. When a critical solid concentration is reached at the locking point, the drops solidify, and the resulting wet particles continue to dry without changing their size during the so-called second drying stage [13]. To account for the change in granule size and composition, the state of the droplets and particles is modeled by a two-dimensional population balance approach, accounting for the different granule sizes and solvent mass fractions. In total three different phases/regions are considered: gas (index G), granules, i.e., drops and particles (index P), and wall (index W).

2.1.1 Gas Phase

Due to the complexity of the fluid dynamics of the gas, a quasi-stationary description for the dry gas (index g) and water vapor (index v) components was chosen as follows:

$$\frac{\mathrm{d}m_{\mathrm{G,g}}}{\mathrm{d}t} \equiv 0 = \dot{m}_{\mathrm{G,g,in}} - \dot{m}_{\mathrm{G,g,out}} \tag{1}$$

$$\frac{\mathrm{d}m_{\mathrm{G,v}}}{\mathrm{d}t} \equiv 0 = \dot{m}_{\mathrm{G,v,in}} - \dot{m}_{\mathrm{G,v,out}} + \dot{m}_{\mathrm{v,P}\to\mathrm{G}} \tag{2}$$

The mass flows of the different components at the inlet and the outlet is given by $\dot{m}_{\mathrm{G,in/out}}$ and the transfer flow of the water vapor between the granule and the gas phase by $\dot{m}_{\mathrm{v,P}\to\mathrm{G}}$.

The enthalpy balance is used to determine the gas temperature and accounts for heat transfer with granular phase and the wall as well as the enthalpy flow from the evaporation mass flow as follows:

$$\begin{aligned}\frac{\mathrm{d}H_{\mathrm{G}}}{\mathrm{d}t} &= \frac{\mathrm{d}(m_{\mathrm{G}}h_{\mathrm{G}})}{\mathrm{d}t} \equiv 0 \\ &= \dot{m}_{\mathrm{G,in}}h_{\mathrm{G,in}} - \dot{m}_{\mathrm{G,out}}h_{\mathrm{G}} + \dot{H}_{\mathrm{v,P}\to\mathrm{G}} - \dot{Q}_{\mathrm{G}\to\mathrm{P}} - \dot{Q}_{\mathrm{G}\to\mathrm{W}}\end{aligned} \tag{3}$$

where $h_{\mathrm{G}} = f(T_{\mathrm{G}})$ is the specific enthalpy of the respective entity, $\dot{H}_{\mathrm{v,P}\to\mathrm{G}}$ is the enthalpy flow of the evaporated water vapor, $\dot{Q}_{\mathrm{G}\to\mathrm{P}}$ and $\dot{Q}_{\mathrm{G}\to\mathrm{W}}$ are the heat flows that are transferred between the gas granular phase and wall, respectively.

2.1.2 Granular Phase

The granular phase consists of both droplets and solidified particles that are present in the domain. To account for varying granule sizes and water contents during the evaporation process, a mass-based two-dimensional population balance approach is developed. Fig. 1 shows the two-dimensional grid for the size and moisture classes, on which the population balances are applied. According to the beforementioned drying stages, three different granule states are considered, as exemplary depicted in Fig. 1a, drop, solidified moist particle and dry solid particle. The state of the granule is determined by the water mass fraction of respective population. Figs. 1b–d illustrate the implementation of the size and composition changes of the granule populations due to evaporation. For droplets, the size and water mass fraction decrease when water is evaporated, leading to a diagonal

granule mass flow towards a population class with a lower particle size and water mass fraction, as shown in Fig. 1c. A solidified particle shows only a decrease in water mass fraction, leading to a mass transfer against the water mass fraction axis as shown in Fig. 1d. Dry solidified particles are treated as inert with respect to the evaporation mechanisms.

A population mass balance for size class i and moisture class j reads as follows:

$$\frac{\mathrm{d}m_{\mathrm{P,i,j}}}{\mathrm{d}t} = \dot{m}_{\mathrm{P,in,i,j}} - \dot{m}_{\mathrm{P,out,i,j}} + \dot{m}_{\mathrm{P,evap,in,i,j}} - \dot{m}_{\mathrm{P,evap,out,i,j}} \quad (4)$$

where $\dot{m}_{\mathrm{P,in/out}}$ are the particle mass flows into and out of the spray dryer calculation domain and $\dot{m}_{\mathrm{P,evap,in/out}}$ are the particle mass flows across the population classes due to the evaporation process as shown in Fig. 1. The difference of the sums over the incoming and outgoing particle mass flows due to evaporation leads to the total evaporated water mass flow entering the gas phase.

For the particle phase, the temperature is averaged over all population classes, i.e., an overall enthalpy balance of the particle balance, is solved as follows:

$$\frac{\mathrm{d}H_{\mathrm{P}}}{\mathrm{d}t} = \frac{\mathrm{d}(m_{\mathrm{P}}h_{\mathrm{P}})}{\mathrm{d}t} = \dot{m}_{\mathrm{P,in}}h_{\mathrm{P,in}} - \dot{m}_{\mathrm{P,out}}h_{\mathrm{P}} - \dot{H}_{\mathrm{v,P}\to\mathrm{G}} + \dot{Q}_{\mathrm{G}\to\mathrm{P}} \quad (5)$$

The average temperature of the granule phase T_{P} is calculated analogously to the gas phase from the specific enthalpy h_{P}. The enthalpy flow $\dot{H}_{\mathrm{v,P}\to\mathrm{G}}$ corresponds to vapor mass flow that is transferred to the gas phase and $\dot{Q}_{\mathrm{G}\to\mathrm{P}}$ is the total heat exchange flow between gas and granular phase.

2.1.3 Transfer Flows

The heat and mass transfer between granular and gas phase depends strongly on the granular size distribution, as smaller granules have a larger specific surface area than larger ones. Following correlations are used:

$$\dot{m}_{\mathrm{v,P}\to\mathrm{G}} = \sum_{\mathrm{i}}\sum_{\mathrm{j}} \dot{m}_{\mathrm{v,P}\to\mathrm{G,i,j}} = \sum_{\mathrm{i}}\sum_{\mathrm{j}} A_{\mathrm{i,j}}\beta_{\mathrm{i,j}}(Sh)\left(Y_{\mathrm{v,sat}}(T_{\mathrm{P}}) - Y_{\mathrm{v,G}}\right) \quad (6)$$

$$\dot{Q}_{\mathrm{G}\to\mathrm{P}} = \sum_{\mathrm{i}}\sum_{\mathrm{j}} \dot{Q}_{\mathrm{G}\to\mathrm{P,i,j}} = \sum_{\mathrm{i}}\sum_{\mathrm{j}} A_{\mathrm{i,j}}\alpha_{\mathrm{i,j}}(Nu)(T_{\mathrm{G}} - T_{\mathrm{P}}) \quad (7)$$

Here, $A_{\mathrm{i,j}}$ is the surface area, $\beta_{\mathrm{i,j}}$ the mass transfer coefficient and $\alpha_{\mathrm{i,j}}$ the heat transfer coefficient of granules in size class i and moisture class j, $Y_{\mathrm{v,sat}}(T_{\mathrm{P}})$ is the vapor saturation concentration at the particle surface and $Y_{\mathrm{v,G}}$ the vapor concentration in the gas phase. The vapor saturation concentration is calculated using the saturation pressure according to the Antoine equation [14]. The heat and mass transfer coefficient are calculated using the Ranz-Marshall correlation for the Nusselt number Nu and Sherwood number Sh for single droplet evaporation [15].

The particle mass transfer between the population classes depends on the respective $\dot{m}_{\mathrm{v,P}\to\mathrm{G,i,j}}$ and the target size and water mass fraction of the receiving class as follows:

$$\dot{m}_{\mathrm{P,evap,out,i,j}} = \frac{\dot{m}_{\mathrm{v,P}\to\mathrm{G,i,j}}}{m_{\mathrm{single,w,i,j}} - m_{\mathrm{single,w,k,l}}} m_{\mathrm{single,i,j}} \quad (8)$$

where $m_{\mathrm{single,w,i,j}}$ is the water mass in a single granule of size class i and moisture class j. The

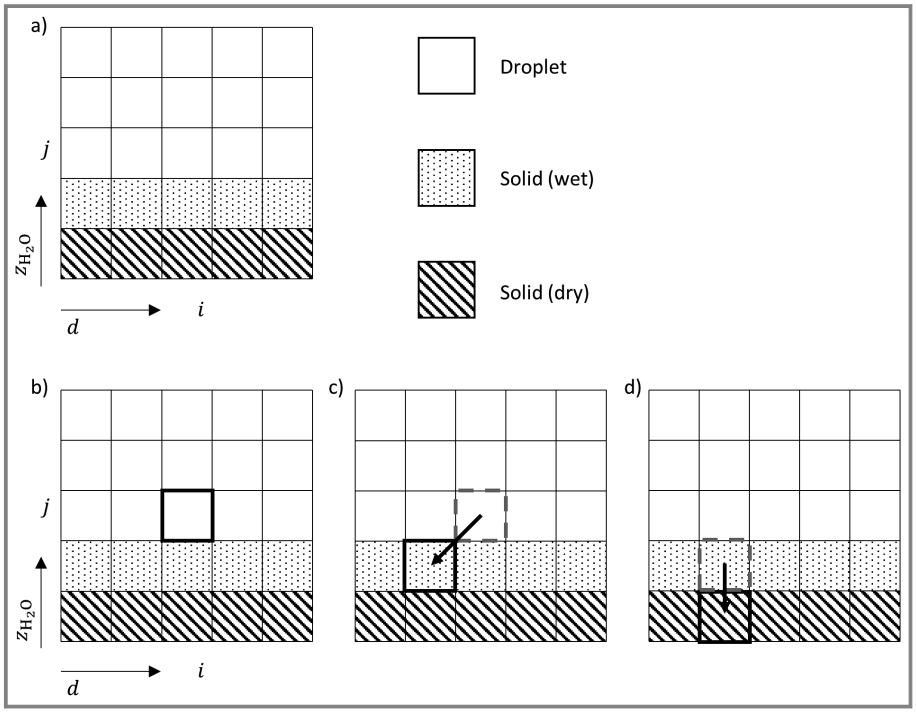

Figure 1. a) Two-dimensional population balance description for the spray dryer model depending on the granule size and the water mass fraction. b) Exemplary granule population in size class i and moisture class j. c) Droplet state drying leads to a decrease in size and water mass fraction. d) Wet solid particle drying leads only to decrease in water mass fraction while the particle size stays fixed.

index variables k and l denote the indices of the target size and moisture classes, according to the illustration in Fig. 1.

The heat exchange with the environment $\dot{Q}_{G\rightarrow W}$ is calculated by assumption of free convection on the outside wall, according to [16].

2.2 Fluidized Bed

The model for the bubbling fluidized bed dryers comprises a hydrodynamic model to determine the size of bubbles and the whereabouts of solids in the unit. Based on that, the heat and mass transfer between bubble gas, suspension gas and solid product to-be-dried is calculated by the drying model.

2.2.1 Hydrodynamic Model Part

The fluidized bed hydrodynamics is modeled considering a dense bottom zone, which comprises solid free bubbles and a suspension phase from gas and solids. The height of the dense bottom zone is determined by the bubble volume fraction, the bubble mean diameter as well as the bubble rise velocity. These values vary along the dryer height. Thus, the fluidized bed is discretized in height elements and the values are calculated along the reactor height. Above the dense bubbling phase, a dilute upper zone is considered. This zone is characterized by elutriation of particles from the dense zone. The implementation of the applied hydrodynamic model is described by Puettmann et al. [17]. The model in this work additionally allows for the transient change of the bed mass inside the dryer, leading to changes in the operation parameters (u_0, $T_{g,in}$). This will alter the fluidized bed holdup mass m_s, the bed height and the solids concentration c_v of the zones in the fluidized bed.

$$\frac{dm_s}{dt} = \dot{m}_{s,in}(t) + \dot{m}_{s,out}\left[m_s(t), c_v(t),\ u_0(t),\ T_{g,in}(t)\right] \quad (9)$$

The dynamic framework of the fluidized bed hydrodynamics was described in Haus et al. [18].

2.2.2 Drying Model Part

The drying model equations by Lai et al. [8] are used to describe the heat and mass transfer between bubbles and suspension as well as the evaporation of water from the particles. The heat and mass transfer system used in this work is depicted in Fig. 2.

To model the transient behavior of the moisture content, the general change of water over time inside the fluidized bed dryer is calculated as follows:

$$\frac{dm_w}{dt} = \dot{m}_{s,in}X_{s,in} - \dot{m}_{s,out}X_{s,\,bed} - \dot{m}_{w,evap} \quad (10)$$

3 Experimental and Simulation Setup

3.1 Pilot-scale Spray Dryer

A pilot-scale spray dryer was operated for the validation of the spray dryer model using standard fumed silica particle suspensions dispersed in water as a reference material. A suspension mass flow of 156 kg h^{-1} with an initial solid concentration of 30 wt % was used. The spray dryer has a height of 10 m and a diameter of 1.5 m. For the atomization, a two-fluid nozzle, operated at 1.75 bar, was used at a gas-to-liquid ratio of 0.4. The estimated mean drop diameter is at 100 µm. A drying gas flow of 1500 Nm^{3}h^{-1} at 200 °C was applied.

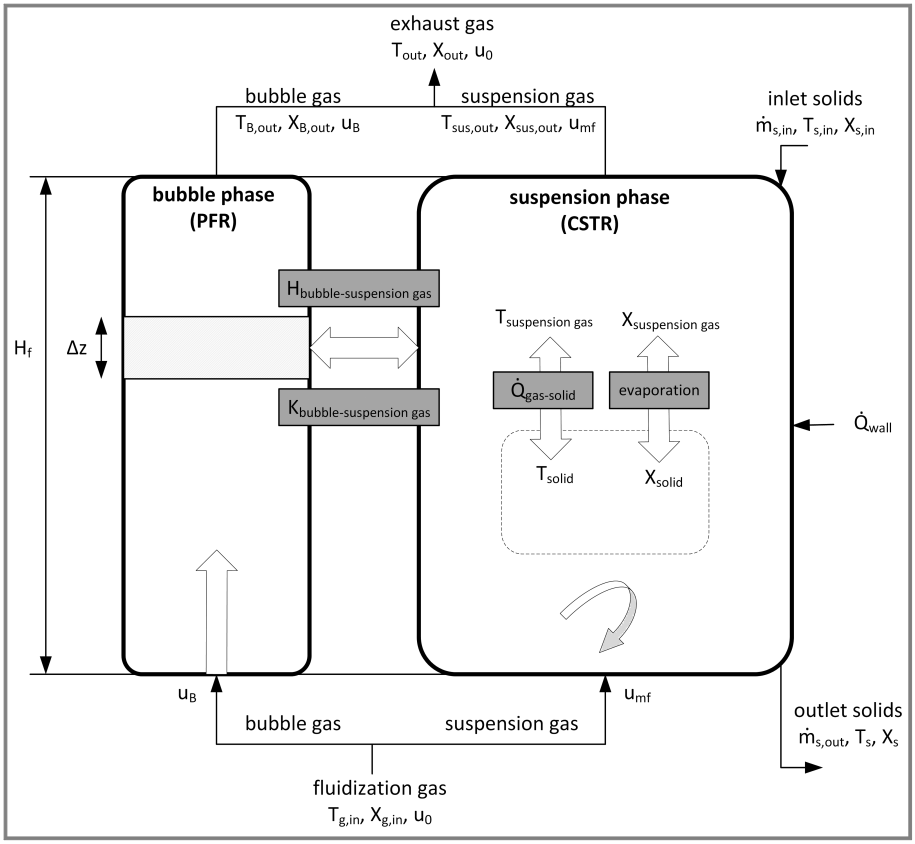

Figure 2. Model of heat and mass exchange in the fluidized bed dryer.

3.2 Lab-scale Fluidized Bed

A lab-scale fluidized bed, as shown in Fig. 3, was operated to achieve information on the drying behavior for the material. The fluidized bed is operated at an inlet temperature between 60 °C and 70 °C. The superficial gas velocity of the fluidization gas flow was arranged with a flow control meter. The material has a bulk density of 700 kg m^{-3}, an average particle diameter of 400 µm and a heat capacity of 1.5 J kg^{-1} K^{-1}. 200 g of wet material with an initial water mass fraction of 40 wt %, corresponding to a moisture content of 0.67 g g_{dry}^{-1}, was used. The varied operational conditions of the experimental runs are shown in Tab. 1.

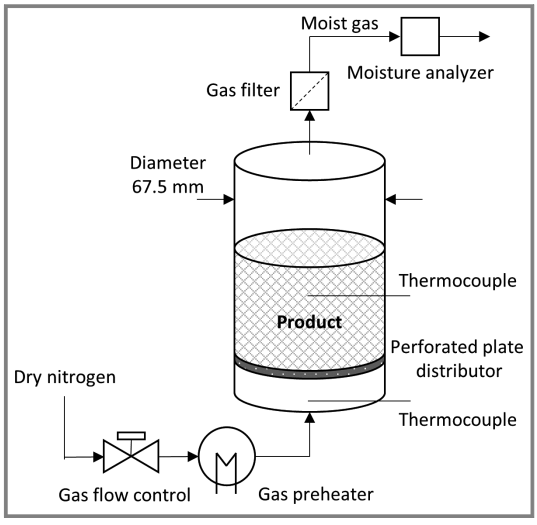

Figure 3. Lab-scale fluidized bed kinetic reactor as operated at BASF for the determination of the drying kinetics.

During fluidization, the bed had a height of around 100 mm, and a fixed bed height of around 80 mm. Thermocouples measured the temperature of the inlet gas and inside the fluidized bed drying chamber. The outlet gas flow is analyzed for the relative humidity at a set temperature.

3.3 Multistage Dryer

In a first step, the presented fluidized bed dryer model is fitted to the batch experiments in the lab-scale fluidized bed reactor as shown in Fig. 4 where stream (1) on the left represents the gas inlet and stream (2) the outlet gas. The operation input parameters in the simulation were set exactly as in the lab runs as described before. By accurately meeting the drying behavior seen in the experiments, the drying parameters n and K as well as the critical moisture content of the product are extracted.

Table 1. Experimental runs for drying parameter adjustment.

Run	1	2	3
T_{in} [°C]	60	60	70
u_0 [m s^{-1}]	0.25	0.125	0.25

The extracted parameters for the drying kinetics were then used for the dynamic simulation of a small industrial scale and continuous process shown on the right side in Fig. 4. Stream (1) is introducing 250 kg h^{-1} of spray suspension into the spray tower with an inlet moisture of 50 wt % water, corresponding to a moisture content of 1 g g_{dry}^{-1}. Drying gas is introduced to the spray dryer via inlet stream (2). The partly dried product with a moisture of around 40 wt % enters the fluidized bed stage in stream (3). The three fluidized bed chambers are fluidized with streams (4), (7) and (10) and should establish a superficial gas velocity of 0.25 m s^{-1}. A difference compared to the lab-scale trials arises, because ambient air is used in the industrial process with an inlet moisture content of 8 g kg_{dry}^{-1}. Both the spray dryer as well as the fluidized bed unit models allow for a starting inlet moisture content, which will influence the drying behavior of the material.

The aim of the small industrial scale simulation is to find suitable dimensions of the spray column and the chambered fluidized bed to achieve a final outlet moisture content below 5 wt % water in the product.

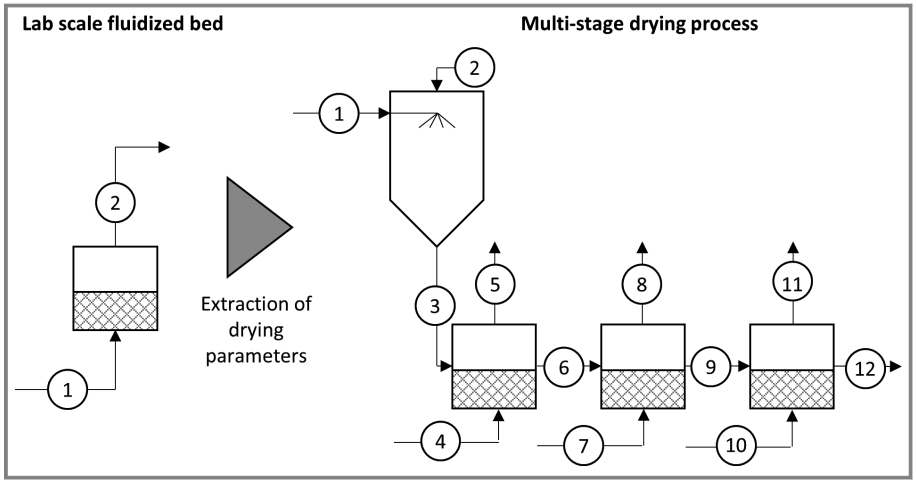

Figure 4. Workflow and flowsheets of the lab-scale fluidized bed and the small industrial scale process comprising a spray tower, a chambered fluidized bed with three consecutive beds.

4 Simulation Results

4.1 Spray Dryer

The pilot-scale spray dryer setup, described in Sect. 3.1, was used to validate the presented spray dryer model. The time series of solid mass flow and solid mass fraction of the granules are shown in Fig. 5a. Over time the initially empty drying chamber fills with granules leading to an increase of the solids in the drying chamber. A mean residence time of the granules $\tau = m_P/\dot{m}_P$ is estimated with a value of 20 s due to the plant operation conditions. As the solids heat up and the water evaporates, the solid mass fraction increases resulting in a final solid mass fraction of 96.3 %, which is in good agreement with the measured product solid mass fractions of 98.0 %. Due to the quasi-stationary model, the simulated gas temperature rapidly changes its state to a constant value of 99.5 °C, while a gas temperature of 100 °C was measured, with an elevated moisture content of 3.78 g g_{dry}^{-1} due to the uptake of the evaporated water from the suspension. The computed Q_3 distributions of the product particles in Fig. 5c show a decrease in particle sizes over time, representing the decreasing droplet sizes due to evaporation until a steady state is reached. The comparison of the computed final particle size distributions from the pilot plant product are in very good agreement, suggesting a fitting model structure for the spray drying process.

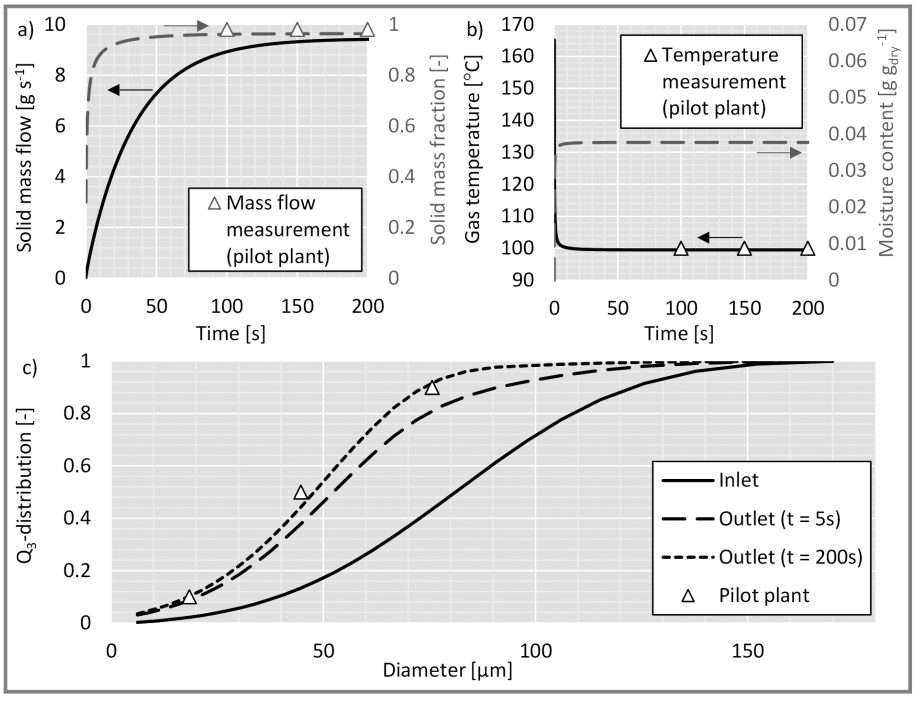

Figure 5. Results of spray dryer simulation at the outlet: a) Solid mass flow (solid line) and solid mass fraction over time (dashed line). b) Gas temperature (solid line) and moisture content of gas flow (dashed line) over time. c) Comparison of granule size distribution at the spray dryer outlet at different time points with measurements from a pilot-scale plant.

4.2 Lab-scale Fluidized Bed

As described in Sect. 3.2, three different experimental runs were used for the calibration of the drying parameters. As the presented models showed deviations from the measurements for the implemented fluid and the thermodynamic models, a calibration of the applied heat and mass transfer coefficients $K_{\text{bubble-suspension}}$ and $H_{\text{bubble-suspension}}$, that are shown in Fig. 2, had to be performed to match the temperature measurements inside the fluidized bed. Afterwards the drying parameters n and K could be adjusted according to the measurements of the moisture content. The resulting time series of the particle temperatures and the particle moisture contents inside the fluidized bed are shown in Fig. 6, for the set of model parameters that is given in Tab. 2.

Table 2. Fitted values of model parameters to the measurements from lab scale fluidized bed experiments.

Parameter	Fitted value
$K_{\text{bubble-suspension}}$	6
$H_{\text{bubble-suspension}}$	6
n	3
K	0.001

The time series of the particle moistures are in good agreement with the measurements allowing for a subsequent usage of the drying parameters n and K for the following design simulation of the multistage drying process. The deviations in the particle temperatures can be mainly accounted to the thermal inertia of the wall that is heated up in the experiments, which is not considered in the fluidized bed model.

4.3 Multistage Drying Process

With the validated models for the spray tower and the fluidized bed dryer, a multistage industrial process was simulated. The plant dimensions were altered to meet the final target, a moisture content of 5 wt % water of the final product. This led to a spray tower with 2 m in diameter and 6 m

height. Three subsequent fluidized beds with a width of 1,6 m and a depth of 1 m each were enough to reach the target. A weir height of 0.25 m was rendered a good option for the fluidized bed reactors.

Fig. 7a shows the mass flows after each drying stage. The particles exit the spray tower with 0.46 kg s^{-1} and a temperature of 23 °C as shown in Fig. 7b and a water mass fraction of around 40 wt % given in Fig. 7c. The mass flow from the first fluidized bed dryer starts at 0 kg s^{-1}, but after filling up to the weir height it goes up to 0.45 kg s^{-1} and stabilizes towards a steady outflow of 0.40 kg s^{-1}. The decrease in mass flow in comparison with the mass flow of the spray dryer outlet is due to the lower moisture content of the particles. The second stage again starts with no outflow towards stage 3. After around 1.5 h particles amounting to 0.31 kg s^{-1} exit the bed towards stage 3 with a water mass fraction of 0.12 wt %. In the third stage the final drying towards 0.047 wt % water is established, and a mass flow of 0.29 kg s^{-1} is achieved, which corresponds to a total product mass flow of 100 $kg_{dry}h^{-1}$. The bed temperatures stabilize at 26 °C in stage 1, to 29 °C in stage 2 and reach 51 °C at the exit of stage 3.

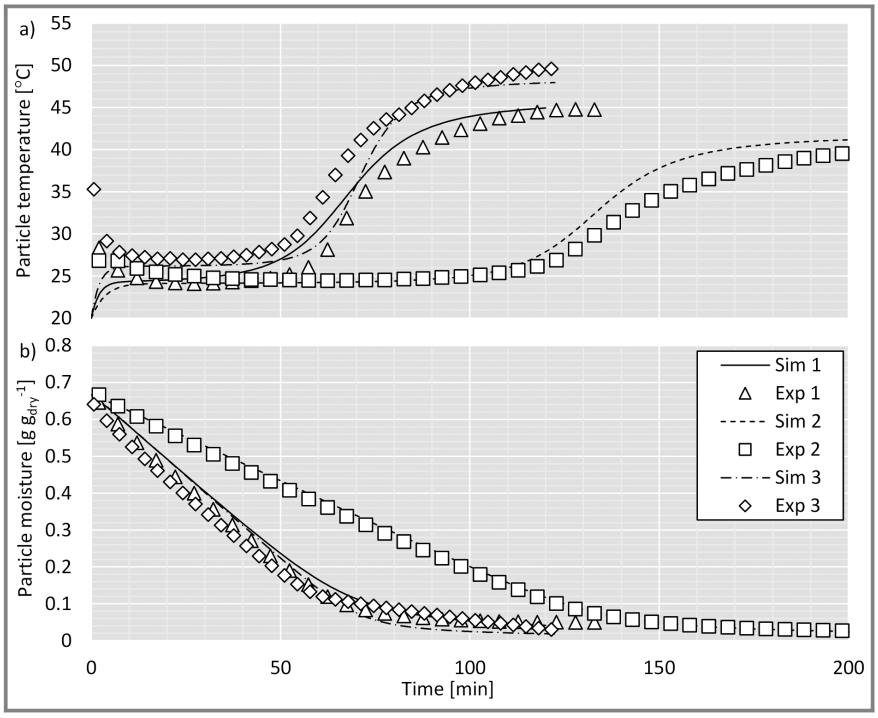

Figure 6. a) Time series of the particle temperatures for experiments corresponding simulations. b) Respective time series of the moisture content of the particles inside the fluidized bed.

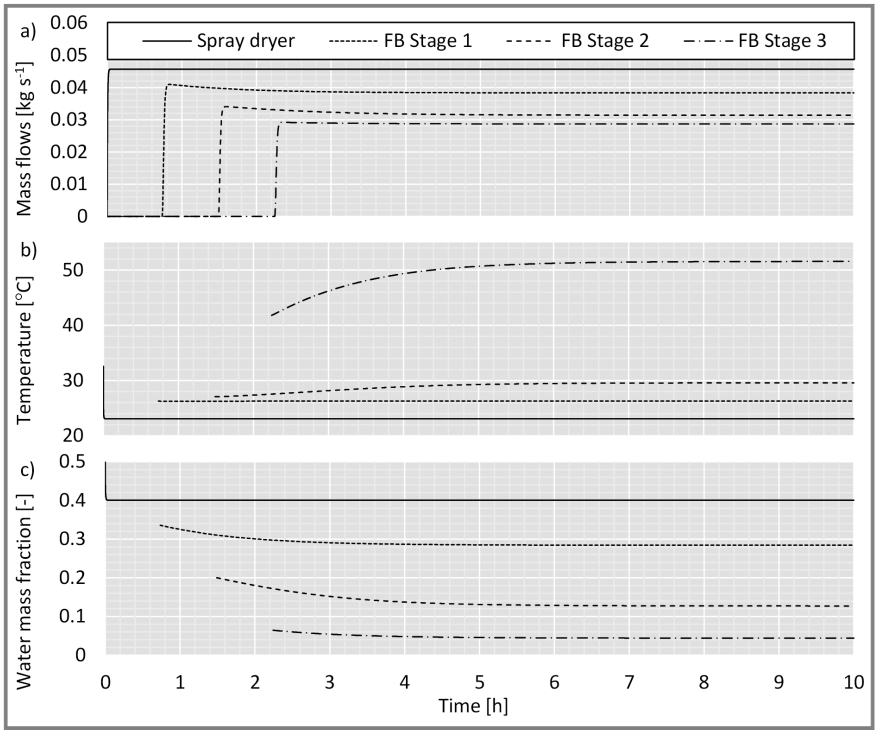

Figure 7. Simulation results for the solid streams at the outlet of the different process stages: a) Solid phase mass flows, b) solid phase temperatures and c) solid phase water mass fraction. The temperatures and water mass fractions of for the time points at which the mass flow is zero are not included.

5 Conclusion

In this contribution, a dynamic spray dryer model based on two-dimensional population balances is introduced. The model allows for the calculation of the transient behavior of the evaporation leading to changes in particle sizes that may have different moisture contents. A comparison with the results of a pilot-scale spray dryer shows the suitability of this approach. Furthermore, a dynamic model of a fluidized bed is presented considering both the hydrodynamic and thermodynamic mechanisms inside the drying chamber. The fluidized bed model is validated using lab-scale experimental data that are also used for the determination of the

drying kinetics. These calibrated models are then applied to create a flowsheet model of a multistage drying process, which is used as a tool to design the dimensions of the single unit operations.

Open access funding enabled and organized by Projekt DEAL.

Symbols used

A	[m^2]	surface area
c_v	[$kg\,m^{-3}$]	solids concentration
d	[m]	granule diameter
H	[J]	enthalpy
h	[$J\,kg^{-1}$]	specific enthalpy
$\dot{H}$	[W]	enthalpy flow
m	[kg]	mass
$\dot{m}$	[$kg\,s^{-1}$]	mass flow
Nu	[–]	Nusselt number
$\dot{Q}$	[W]	heat flow
Sh	[–]	Sherwood number
T	[K]	temperature
U	[$W\,K^{-1}$]	thermal transmittance
u_0	[$m\,s^{-1}$]	superficial velocity
Y	[$kg\,m^{-3}$]	gas concentration

Greek letters

α	[$W\,m^{-2}K^{-1}$]	heat transfer coefficient
β	[$kg\,m^{-3}$]	gas concentration

Sub- and Superscripts

B	bubble phase
dry	dry matter (gas/solid)
G	gas phase
g	dry gas compound
P	granular particle/drop phase
s	dry solid compound
sus	suspension phase
v	water (vapor)
w	water (liquid)
single	single particle

References

[1] V. Skorych, M. Dosta, E.-U. Hartge, S. Heinrich, *Powder Technol.* **2017**, *314*, 665–679. DOI: https://doi.org/10.1016/j.powtec.2017.01.061
[2] V. Skorych, M. Buchholz, M. Dosta, S. Heinrich, in *Dynamic Flowsheet Simulation of Solids Processes* (Ed: S. Heinrich), Springer International Publishing, Cham **2020**.
[3] V. S. Birchal, M. L. Passos, *Braz. J. Chem. Eng.* **2005**, *22 (2)*, 293–302. DOI: https://doi.org/10.1590/S0104-66322005000200018
[4] L. Norbert Petersen, N. Kjølstad Poulsen, H. H. Niemann, C. Utzen, J. B. Jørgensen, *IFAC Proc. Vol.* **2013**, *46 (32)*, 559–564. DOI: https://doi.org/10.3182/20131218-3-IN-2045.00118
[5] M. Ali, T. Mahmud, P. J. Heggs, M. Ghadiri, D. Djurdjevic, H. Ahmadian, L. M. de Juan, C. Amador, A. Bayly, *Chem. Eng. Res. Des.* **2014**, *92 (5)*, 826–841. DOI: https://doi.org/10.1016/j.cherd.2013.08.010
[6] V. Gnielinski, A. Mersmann, F. Thurner, *Verdampfung, Kristallisation, Trocknung*, Springer, Berlin **1993**.
[7] B. Paláncz, *Chem. Eng. Sci.* **1983**, *38 (7)*, 1045–1059. DOI: https://doi.org/10.1016/0009-2509(83)80026-8
[8] F. S. Lai, Y. Chen, L. T. Fan, *Chem. Eng. Sci.* **1986**, *41 (9)*, 2419–2430. DOI: https://doi.org/10.1016/0009-2509(86)85092-8
[9] L. Garnavi, N. Kasiri, S. H. Hashemabadi, *Int. Commun. Heat Mass Transfer* **2006**, *33 (5)*, 666–675. DOI: https://doi.org/10.1016/j.icheatmasstransfer.2006.02.014
[10] J. Burgschweiger, E. Tsotsas, *Chem. Eng. Sci.* **2002**, *57 (24)*, 5021–5038. DOI: https://doi.org/10.1016/S0009-2509(02)00424-4
[11] M. Peglow, U. Cunäus, E. Tsotsas, *Chem. Eng. Sci.* **2011**, *66 (9)*, 1916–1922. DOI: https://doi.org/10.1016/j.ces.2011.01.041
[12] I. Alaathar, *Fließschema-Simulation der kontinuierlichen Wirbelschichttrocknung mit verteilten Parametern*, 1st ed., SPE-Schriftenreihe, Cuvillier Verlag, Göttingen **2017**.
[13] E. Tsotsas, *Drying Technol.* **2012**, *30 (11–12)*, 1167–1175. DOI: https://doi.org/10.1080/07373937.2012.685139
[14] A. L. Yarin, G. Brenn, O. Kastner, D. Rensink, C. Tropea, *J. Fluid Mech.* **1999**, *399*, 151–204. DOI: https://doi.org/10.1017/S0022112099006266
[15] W. E. Ranz, W. R. Marshall, *Chem. Eng. Prog.* **1952**, *48*, 141–148; 173–180.
[16] *VDI-Wärmeatlas*, 11th ed., Springer Vieweg, Berlin **2013**.
[17] A. Püttmann, E.-U. Hartge, J. Werther, in *Circulating Fluidized Bed Technology IX* (Eds: J. Werther, W. Nowak, K.-E. Wirth, E.-U. Hartge), TuTech Innovation GmbH, Hamburg **2008**.
[18] J. Haus, E.-U. Hartge, S. Heinrich, J. Werther, *Powder Technol.* **2017**, *316*, 628–640. DOI: https://doi.org/10.1016/j.powtec.2016.12.022

DOI: 10.1002/cite.202000207

Process Design of a Multistage Drying Process via Flowsheet Simulation

M. Buchholz, J. Haus, L. Blesinger, C. Riemann, S. Pietsch, F. Kleine Jäger, S. Heinrich*

Research Article: A multistage drying process consisting of a spray dryer and fluidized beds is designed using flowsheet simulation. A novel modeling approach is presented for the spray drying. The dynamic modeling of the fluidized bed is based on an adaptation of established models.